JACS
JOURNAL OF THE AMERICAN CHEMICAL SOCIETY

ARTICLE

pubs.acs.org/JACS

Temperature Dependence of Spin-Selective Charge Transfer Pathways in Donor−Bridge−Acceptor Molecules with Oligomeric Fluorenone and *p*-Phenylethynylene Bridges

Amy M. Scott and Michael R. Wasielewski*

Department of Chemistry and Argonne-Northwestern Solar Energy Research (ANSER) Center, Northwestern University, Evanston, Illinois 60208-3113, United States

Supporting Information

ABSTRACT: The temperature dependence of spin-selective intramolecular charge recombination (CR) in a series of 2,7-fluorenone (FN_{1-2}) and *p*-phenylethynylene ($PE_{1-2}P$) linked donor−bridge−acceptor molecules with a 3,5-dimethyl-4-(9-anthracenyl) julolidine (DMJ−An) electron donor and a naphthalene-1,8:4,5-bis(dicarboximide) (NI) acceptor was studied using nanosecond transient absorption spectroscopy in the presence of a static magnetic field. Photoexcitation of DMJ−An into its charge transfer band and subsequent electron transfer to NI results in a nearly quantitative yield of $^1(DMJ^{+\bullet}-An-FN_n-NI^{-\bullet})$ and $^1(DMJ^{+\bullet}-An-PE_nP-NI^{-\bullet})$, which undergo rapid radical pair intersystem crossing (RP-ISC) to produce the triplet RPs, $^3(DMJ^{+\bullet}-An-FN_n-NI^{-\bullet})$ and $^3(DMJ^{+\bullet}-An-PE_nP-NI^{-\bullet})$, respectively. The CR rate constants, k_{CR}, in toluene were measured over a temperature range from 270 to 350 K, and a kinetic analysis of k_{CR} in the presence of an applied static magnetic field was used to extract the singlet and triplet charge recombination rate constants, k_{CRS} and k_{CRT}, respectively, as well as the intersystem crossing rate constant, k_{ST}. Plots of ln $(kT^{1/2})$ versus $1/T$ for PE_1P show a distinct crossover at 300 K from a temperature-independent singlet CR pathway to a triplet CR pathway that is positively activated with a barrier of 1047 ± 170 cm^{-1}. The singlet CR pathway via the FN_1 bridge displays a negative activation energy that results from donor−bridge and bridge−acceptor torsional motions about the single bonds joining them. In contrast, the triplet CR pathway via the FN_{1-2} and $PE_{1-2}P$ bridges exhibits positive activation energies. The activation barriers to these torsional motions range from 1100 to 4500 cm^{-1} and can be modeled by semiclassical electron transfer theory.

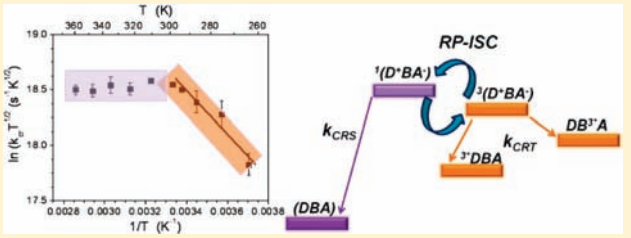

INTRODUCTION

The rational design of organic materials that convert photon energy into electrical energy is of great interest in solar cell design. Nature already possesses an optimized mechanism for solar energy conversion and storage in well-ordered assemblies of photofunctional chromophores in photosynthetic plants and bacteria.[1] Efficient photodriven charge separation (CS) reactions to form long-lived radical pairs (RPs) within specifically tailored nanoenvironments are key energy transduction processes that occur in photosynthetic reaction center proteins.[2] Emulating these processes in photofunctional donor−bridge−acceptor (D−B−A) molecules is important for developing new molecules and materials for solar energy conversion, so that the details of how the most favorable charge transport mechanisms depend on molecular structure are of great experimental and theoretical interest.[3−5]

Electronic coupling, environment (solvent and temperature), and energetics are all parameters that dramatically influence the lifetime of RPs and, consequently, the charge transport mechanism in D−B−A systems. Bridge-mediated charge transport by the superexchange mechanism involves mixing of bridge states with those of the donor and acceptor and requires that the bridge states have energies that are higher than and well-separated from those of the donor. This results in an exponential dependence of the charge transport rate constant on distance, eq 1:

$$k = k_0 e^{-\beta(r - r_0)} \quad (1)$$

where k_0 is the rate constant at the van der Waals contact distance r_0 (3.5 Å), and β is the damping coefficient for the decay. A more efficient means of transporting charge used by photosynthetic systems is the charge hopping mechanism,[6−8] which occurs by a change in redox state of the molecular bridge because of small charge injection barriers between D−B and B−A. The distance dependence for charge hopping is weak, $1/r^n$, where $n = 2$ for an unbiased random walk and trends toward $n = 1$ for a CR recombination reaction biased by Coulomb attraction of the opposite charges.[9] This distinguishing factor is often used to identify the transition from superexchange to a hopping mechanism in distance-dependent charge transfer rate measurements. However, lengthening the bridge often changes other system parameters, such as bridge redox potentials and molecular conformations.[10] Charge transport within π-linked D−B−A molecules has been studied under a variety of conditions[9,11−18]

Received: October 24, 2010
Published: February 14, 2011

dx.doi.org/10.1021/ja1095649 | J. Am. Chem. Soc. 2011, 133, 3005–3013

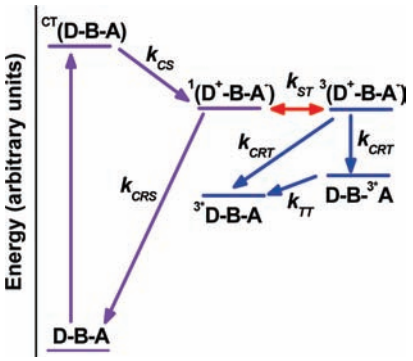

Figure 1. Charge transfer scheme for FN_{1-2} and $PE_{1-2}P$.

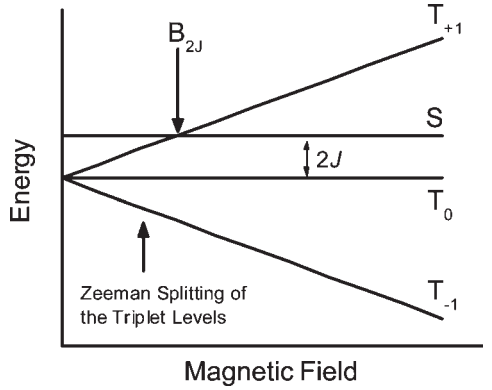

Figure 2. Schematic of radical ion pair energy levels as a function of magnetic field ($2J > 0$).

to identify the molecular properties that determine crossover between superexchange and hopping when molecular systems exhibit a combination of these mechanisms.[19−22]

The temperature dependence of charge transfer rates has been described for many natural and artificial photosynthetic systems with results ranging from the unusual temperature dependence of *Rb. sphaeroides* reaction centers[23] to the temperature-independent rates observed in some D−B−A systems.[24−26] Additionally, the temperature dependencies show that electron transfer rates in the Marcus normal region differ from those in the inverted region,[27] where $|\Delta G| > \lambda$ and nuclear tunneling can dominate. There is also precedence in the literature for thermally activated processes that occur when the energy barrier between sites is lowered by nuclear motion, which has been shown to "gate" the charge transfer when the activation energy is identical to that of the bridge motion.[28−31]

For D−B−A molecules having RP lifetimes longer than a few nanoseconds, magnetic field effect (MFE) experiments on reaction rates and/or product yields have demonstrated that CR frequently occurs by competitive singlet and triplet RP recombination pathways.[32,33] Briefly, the initial photogenerated singlet RP may undergo electron−nuclear hyperfine coupling-induced radical pair intersystem crossing (RP-ISC) to produce the triplet RP, $^1(D^{+\bullet}-B-A^{-\bullet}) \rightarrow {}^3(D^{+\bullet}-B-A^{-\bullet})$. The subsequent CR is spin selective; that is, the singlet RP recombines to the singlet ground state and the triplet RP recombines to yield the neutral local triplet (Figure 1). Application of a static magnetic field causes Zeeman splitting of the RP triplet sublevels, and varying the field strength modulates the efficiency of RP-ISC by adjusting the energies of the RP triplet sublevels relative to that of the

Scheme 1. Donor−Bridge−Acceptor Systems Used in This Study

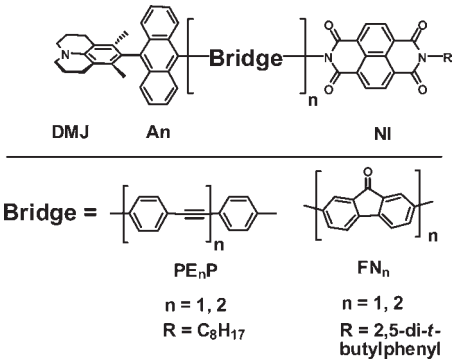

singlet level (Figure 2). When the Zeeman splitting of the triplet RP sublevels equals the intrinsic RP singlet−triplet splitting, $2J$, there is an increase in the RP-ISC rate. This increase translates into a maximum in triplet RP production and therefore a maximum in neutral local triplet yield upon CR. By monitoring the yield of local triplet production as a function of applied magnetic field, the magnitude of $2J$ can be measured directly[34,35] and can be used to estimate V_{DA} because $2J \propto V_{DA}^2$.[36−39] The mechanistic details of the radical pair intersystem crossing mechanism (RP-ISC) and the theory behind MFEs have been researched extensively[40−44] and applied to both biological[45−49] and chemical[36,50−57] donor−acceptor systems.

We have previously reported on photoinduced charge transport in D−B−A systems with 2,7-fluorenone (n = 1−3) (FN_n) and *p*-phenylethynylene (n = 1−3) (PE_nP) molecular bridges covalently attached to a 3,5-dimethyl-4-(9-anthracenyl) julolidine (DMJ-An) electron donor and a naphthalene-1,8:4,5-bis-(dicarboximide) (NI) acceptor (Scheme 1) and have shown that the superexchange mechanism dominates CR.[33] Photoexcitation of DMJ−An produces long-lived singlet RPs $^1(DMJ^{+\bullet}-An-FN_n-NI^{-\bullet})$ and $^1(DMJ^{+\bullet}-An-PE_nP-NI^{-\bullet})$, which undergo RP-ISC to the corresponding triplet RPs with subsequent spin-selective CR to ^{3*}An and ^{3*}NI. Our previous work established that a superexchange mechanism dominates both singlet and triplet CR pathways for the $PE_{1-3}P$ and FN_{1-3} bridges at room temperature. In this work, we examine the temperature dependence of CR for FN_{1-2} and $PE_{1-2}P$ with the aim of identifying the dominant charge transport pathway through the use of nanosecond transient absorption spectroscopy in the presence of an applied static magnetic field. We examine how V_{DA} depends on molecular structure by analyzing the spin−spin exchange interaction ($2J$) between the unpaired spins of the RPs using MFEs. Additionally, we employ a kinetic model to separate the spin-selective charge recombination rate constants, k_{CRS} and k_{CRT}, as a function of temperature by analyzing MFEs on the observed RP and neutral triplet state populations that result from CR.

EXPERIMENTAL SECTION

The synthesis and characterization of the compounds used in this study have been described elsewhere.[32,58] Samples for nanosecond transient absorption spectroscopy were placed in a 10 mm path length quartz cuvette and freeze−pump−thaw degassed five times. The samples were excited with 7 ns, 2.5 mJ, 416 nm laser pulses using the frequency-tripled output of a Continuum Precision II 8000 Nd:YAG

dx.doi.org/10.1021/ja1095649 |*J. Am. Chem. Soc.* 2011, 133, 3005–3013

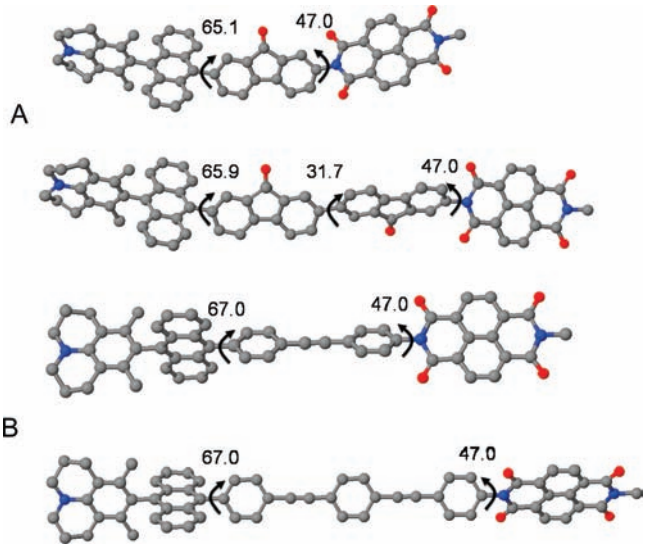

Figure 3. Representative DFT (B3LYP, STO-3G) energy minimized structures for (A) DMJ−An−FN_{1-2}−NI and (B) DMJ−An−$PE_{1-2}P$−NI. The hydrogens are removed in the figure for clarity.

laser pumping a Continuum Panther OPO. The excitation pulse was collimated to a 5 mm diameter spot and matched to the diameter of the probe pulse generated using a xenon flashlamp (EG&G Electro-Optics FX-200). The probe light was collected with a monochromator and photomultiplier tube with high voltage applied to only four dynodes (Hamamatsu R928), and kinetics were recorded with a LeCroy Wavesurfer 42Xs oscilloscope interfaced to a custom Labview program. The total instrument response time is 7 ns and is determined primarily by the laser pulse duration. Analysis of the kinetic data was performed at multiple wavelengths using a Levenberg−Marquardt nonlinear least-squares fit to a general sum-of-exponentials function with a convoluted Gaussian function to account for the finite instrument response.

For the magnetic field effect experiments, the sample cuvette was placed between the poles of a Walker Scientific HV-4W electromagnet powered by a Walker Magnion HS-735 power supply, and the field strength was measured by a Lakeshore gaussmeter with a Hall effect probe. The electromagnet and gaussmeter were interfaced with Labview, allowing measurements and control of the magnetic field to $\pm 1 \times 10^{-5}$ T during the data acquisition. To maintain sample integrity during the experiment, a probe light shutter was used to block the sample from irradiation when transient absorption kinetics were not being collected. The triplet yield was monitored at 480 nm, and kinetic traces were collected in increments of 0.1, 1.5, or 5.0 mT with zero field $\Delta A(B = 0)$ collection after four or five steps. To compensate for possible sample degradation, zero field kinetics were collected during the experiment in four or five step increments and plotted and fit with polynomial or linear trend lines. These functions were used to calculate the relative RP yield or triplet yield as a function of applied field strength (B) and plotted as $\Delta A(B)/\Delta A(B = 0)$. The results presented were conducted on separate days with freshly prepared samples in spectrophotometric or freshly distilled ACS-grade toluene.

For variable temperature nanosecond transient absorption experiments, a thermostatted cuvette cell holder (Quantum Northwest Flash 100) that maintained the temperature at the sample within ±0.1 K was used. The sample was allowed to equilibrate for 30 min prior to each sample run. Accurate MFE experiments for PE_3P and FN_3 using transient absorption detection could not be performed over an analytically useful range of temperatures because k_{CR} is relatively slow, so that very low sample concentrations are required to eliminate intermolecular CR.

Table 1. Parameters for the Fit to the Temperature-Dependent Charge Transfer Rates of FN_{1-2} and $PE_{1-2}P$ in Toluene Extracted from Linear Fits to the Data in Figures 4, 5, 9−11

compound	pathway	range (K)	$\Delta G^{\ddagger}$ (cm^{-1})	A (s^{-1} $K^{1/2}$)	R^2
FN_1	k_{CR}	268−353	−510 ± 21	2.6×10^7	0.927
	k_{CRS}	273−353	−811 ± 147	5.1×10^6	0.884
	k_{CRT}	273−353	1047 ± 170	6.7×10^{10}	0.904
FN_2	k_{CR}	270−350	2248 ± 22	2.2×10^{12}	0.998
	k_{CRS}	270−350	1510 ± 118	2.9×10^{10}	0.998
	k_{CRT}	290−350	4107 ± 227	7.9×10^{13}	0.992
PE_1P	k_{CR}	270−296	1368 ± 285	8.8×10^{10}	0.920
	k_{CRT}	270−350	1268 ± 131	7.6×10^{10}	0.959
PE_2P	k_{CR}	270−350	2133 ± 93	9.6×10^{11}	0.985
	k_{CRS}	270−350	1459 ± 40	1.9×10^{10}	0.997
	k_{CRT}	270−350	2930 ± 378	7.1×10^{12}	0.938

RESULTS

Molecular Structure and Energy Levels. Figure 3 shows the energy minimized structures of FN_{1-2} and $PE_{1-2}P$ calculated in a vacuum using density functional theory (DFT) and the STO-3G basis set using Gaussian 98.[59] The DFT calculations reveal that the HOMOs are localized on the DMJ donor and the LUMOs are confined to the NI acceptor. The torsional angles around the An−FN and An−PE_nP single bonds are ~66° and ~47° for FN_n−NI and PE_nP−NI, respectively. The internal reorganization energies, λ_I, were calculated for CR by performing a single-point calculation (UHF) B3LYP/6-31G* on the radical ions of the donor, bridges, and acceptor in the DFT-optimized ground state and subtracting the self-consistent field (SCF) energy of the relaxed ionic conformation from that of the unrelaxed ground-state conformation (Table S1).[25] This information was used in predicting charge transfer rates using electron transfer theory.[60−62]

Temperature-Dependent Charge Recombination. Nanosecond transient absorption studies on FN_{1-2} and $PE_{1-2}P$ were performed to determine the charge recombination rate constants, k_{CR}, in toluene over a temperature range from 270 to 350 K. Photoexcitation of the donor, DMJ−An, with 7 ns, 416 nm laser pulses produces $DMJ^{+\bullet}$−$An^{-\bullet}$ quantitatively, so that $An^{-\bullet}$ acts as a high potential electron donor. Following rapid CS, the initially formed singlet RPs, $^1(DMJ^{+\bullet}-An-FN_n-NI^{-\bullet})$ and $^1(DMJ^{+\bullet}-An-PE_nP-NI^{-\bullet})$, undergo rapid RP-ISC to produce the triplet RPs, $^3(DMJ^{+\bullet}-An-FN_n-NI^{-\bullet})$ and $^3(DMJ^{+\bullet}-An-PE_nP-NI^{-\bullet})$, respectively. The energy levels of the triplet RP states are above those of ^{3*}An and ^{3*}NI, so that spin-selective CR can occur from the triplet RPs to produce (DMJ−An−FN_n−^{3*}NI) and (DMJ−An−PE_nP−^{3*}NI), respectively (E_T = 2.03 eV),[63,64] as well as (DMJ−^{3*}An−FN_n−NI) and (DMJ−^{3*}An−PE_nP−NI), respectively (E_T = 1.85 eV).[65] When spin-selective CR to ^{3*}NI and ^{3*}An occurs, the broad absorption features at 480 and 430 nm[66] persist on the microsecond time scale and appear as plateaus in the kinetic traces.[32] The decay-associated spectra for the FN_2 and PE_2P bridges at 295 K indicate that CR to both ^{3*}An and ^{3*}NI is limited by the lifetimes of their RPs.[32] The lifetimes obtained by fitting individual kinetic traces match the decay lifetimes from the decay associated spectra at 295 K. The inverse time constant for the decay of $NI^{-\bullet}$ fit at its 480 nm (ε_{480} = 30 000 M^{-1} cm^{-1}) and 610 nm absorption maxima[67] is used to monitor the observed rate constant, k_{CR}.

dx.doi.org/10.1021/ja1095649 |J. Am. Chem. Soc. 2011, 133, 3005–3013

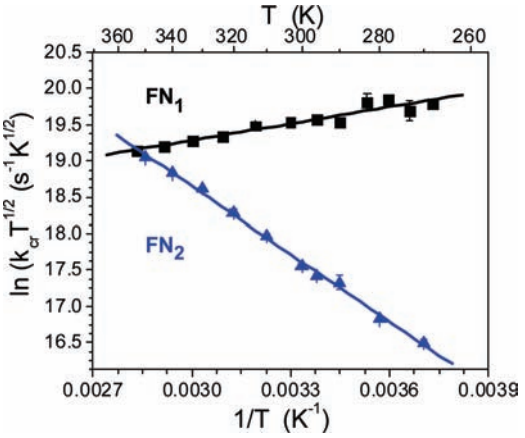

Figure 4. Plot of $\ln[k_{CR}T^{1/2}]$ versus $1/T$ for FN_1 and FN_2 in toluene. Error bars on the data points are smaller than the size of the symbols for all plots, except where given.

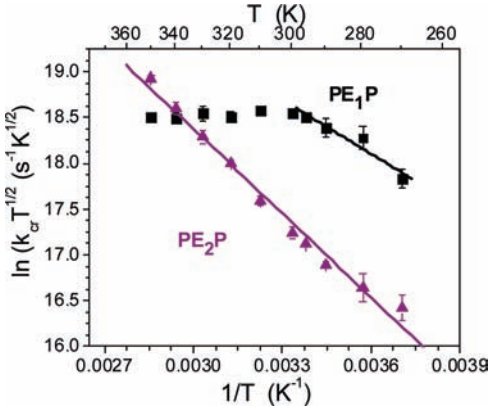

Figure 5. Plot of $\ln[k_{CR}T^{1/2}]$ versus $1/T$ for PE_1P and PE_2P in toluene. Error bars on the data points are smaller than the size of the symbols for all plots, except where given.

The temperature dependence of the rate constants was analyzed using the semiclassical Marcus−Jortner−Hopfield equation for the electron transfer rate in the nonadiabatic limit:[60−62]

$$k_{CR} = \frac{2\pi}{\hbar}|V_{CR}|^2\sqrt{\frac{1}{4\pi\lambda_s k_B T}}\sum_{n=0}^{\infty} e^{(-S)S^n/n!}e^{[-(\Delta G_{CR}+\lambda_s+n\hbar\omega)^2/4\lambda_s k_B T]} \quad (2)$$

where $\hbar\omega$ is the vibrational quantum, assumed to be 1500 cm^{-1}, ΔG_{CR} is the free energy change of radical ion pair recombination, λ_S and λ_I are, respectively, the solvent and internal reorganization energies, and $S = \lambda_I/\hbar\omega$. Because these experiments were performed in the low polarity solvent toluene ($\lambda_S \cong 0.07$ eV), the inner-sphere reorganization, λ_I, dominates the total reorganization energy $\lambda = \lambda_S + \lambda_I$.[32] Given the functional form of eq 2, where $k_{CR} = AT^{-1/2}\exp(-\Delta G^{\ddagger}/k_BT)$, the parameters $\Delta G^{\ddagger}$ and the pre-exponential factor A can be extracted from the slope and intercept of a plot of $\ln(k_{CR}T^{1/2})$ versus $1/T$ (see Table 1).

Plots of $\ln(k_{CR}T^{1/2})$ versus $1/T$ for FN_1 and FN_2 as a function of temperature are given in Figure 4, while the corresponding plots for PE_1P and PE_2P are presented in Figure 5. The results show that the CR rate constant for FN_1 decreases with increasing temperature over the temperature range studied, and the linear

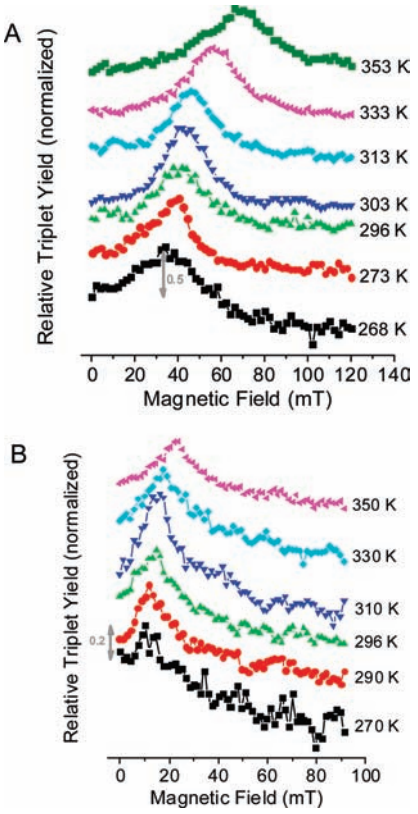

Figure 6. Relative triplet yield versus magnetic field at various temperatures for (A) FN_1 in toluene at 480 nm measured 500 ns after photoexcitation and (B) PE_1P in toluene at 480 nm measured 1 μs after photoexcitation. Curves are offset for clarity and the actual relative triplet yields are given by the grey scale bars.

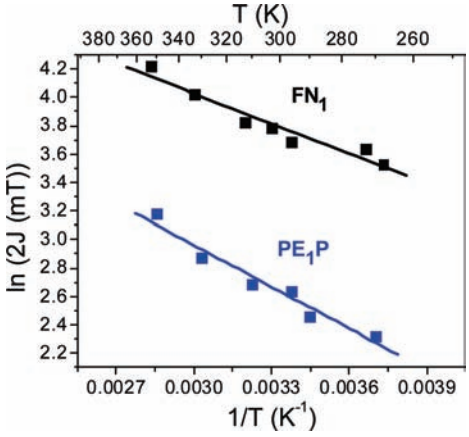

Figure 7. Plot of ln $2J$ versus $1/T$ for FN_1 and PE_1P in toluene, where $2J$ was measured from the MFE peak in Figure 6.

fits give a negative activation barrier, $\Delta G^{\ddagger} = -510 \pm 21$ cm^{-1} ($R^2 = 0.927$). For PE_1P, the rate constant appears to initially increase with temperature, but from 300 to 350 K it becomes temperature independent. The region from 270 to 300 K is fit with a single line that yields a positive activation barrier, $\Delta G^{\ddagger} = 1368 \pm 285$ cm^{-1} ($R^2 = 0.920$). The results for FN_2 and PE_2P both show positive activation barriers over the temperature range studied, with nearly identical values of $\Delta G^{\ddagger}$ close to

dx.doi.org/10.1021/ja1095649 |J. Am. Chem. Soc. 2011, 133, 3005–3013

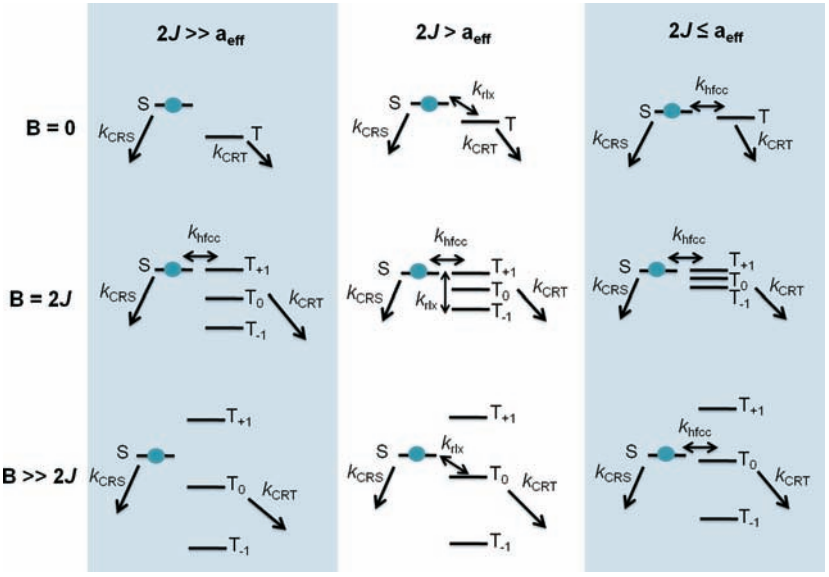

Figure 8. Kinetic model of RP spin dynamics for CR under three conditions, $2J \gg a_{eff}$, $2J > a_{eff}$, and $2J \leq a_{eff}$, when $B = 0$, $B = 2J$, and $B \gg 2J$. The blue dot indicates that initial population resides on the singlet RP (S), and T_{+1}, T_0, T_{-1} denote corresponding spin sublevels with the corresponding rates, k_{CRS} and k_{CRT}, where $k_{ST} = k_{hfcc} + k_{rlx}$.

2100 cm^{-1}. The methods for determining k_{CRS}, k_{CRT}, and k_{ST} will be addressed in the Discussion.

Temperature-Dependent Magnetic Field Effects. The magnetic field effects on the triplet yields for FN_1 and PE_1P are shown as plots of triplet yields (relative to those at $B = 0$) versus magnetic field strength over the temperature range of 270−350 K in Figure 6. The maximum of the relative triplet yield plot, or minimum of the complementary relative RP yield plot (B_{2J}), correspond to the field at which the S and T_{+1} (if $2J > 0$) or T_{-1} (if $2J < 0$) RP energy levels cross. When $B = 2J$, S−T_{+1} mixing occurs because $2J > 0$ at the resonance condition,[32] so that RP-ISC is efficient (Figure 2). These plots show that $2J$ shifts to higher fields as the temperature increases, which most likely results from increased sampling of molecular conformations having stronger electronic coupling.[68] Figure 7 plots ln $2J$ versus $1/T$, which yields linear fits giving activation barriers of 489 ± 57 cm^{-1} ($R^2 = 0.936$) for FN_1 and 680 ± 74 cm^{-1} ($R^2 = 0.956$) for PE_1P. The temperature dependencies of the MFE plots for FN_2 and PE_2P are weak ($2J$ = 3 mT at 295 K, Figure S1).

DISCUSSION

Spin-Selective Charge Recombination. The energy level scheme depicted in Figure 1 shows that CR within the singlet and triplet RP manifolds give different products. The rates at which these products are formed, and consequently their yields, depend on two major considerations. First, spin dynamics controls intersystem crossing and thus population flow between the singlet and triplet manifolds. Following rapid charge separation, the initially formed singlet RP, $^1(D^{+\bullet}-B-A^{-\bullet})$, undergoes radical-pair intersystem crossing (RP-ISC)[69,70] with rate constant k_{ST} induced by electron−nuclear hyperfine coupling within the radicals to produce the triplet RP, $^3(D^{+\bullet}-B-A^{-\bullet})$. The CR reactions take place spin selectively from these RP states, so that interconversion between the singlet and triplet RP states can be a kinetic bottleneck for the overall CR process.[71] Modification of the spin dynamics by an applied magnetic field has been shown to dramatically change the spin-selective RP reaction yields.[43,54,71] These magnetic field effects (MFEs) allow control over the CR lifetime, so that the spin-dependent CR pathways as well as the RP spin−spin exchange interaction $2J$ can be probed.

In general, the overall RP-ISC rate constant $k_{ST} = k_{hfcc} + k_{rlx}$, where k_{hfcc} is the rate constant for S−T_n ($n = 0, \pm 1$) mixing induced by the electron−nuclear hyperfine interaction when the S−T_n energy gap is very small, and k_{rlx} is the total rate constant for all other spin-dependent relaxation processes. Second, the CR rates within the singlet and triplet manifolds depend on the usual considerations of electron transfer theory, that is, the electronic coupling matrix elements, V_{CRS} and V_{CRT}, respectively, as well as the Franck−Condon weighted density of states (FCWD), which includes the reaction free energy and the total reorganization energy, λ, for CR. For example, the free energies of the triplet CR reactions, $^3[D^{+\bullet}-B-A^{-\bullet}] \rightarrow [D-B-^{3*}A]$ or $[^{3*}D-B-A]$, occur near the maximum of the Marcus rate versus free energy profile ($|\Delta G| \cong \lambda \cong 0.5$ eV), while that of the singlet CR reactions $^1[D^{+\bullet}-B-A^{-\bullet}] \rightarrow D-B-A$ occurs far into the Marcus inverted region ($|\Delta G| \cong 2.3$ eV).[60] Thus, the triplet CR rate should be much faster than the singlet CR rate based on FCWD considerations alone. The formation rates and yields of singlet and triplet CR products in $PE_{1-2}P$ and FN_{1-2} are analyzed using these two basic ideas.

A kinetic model based on the RP-ISC mechanism with state-dependent recombination reactions was used to analyze the magnetic field-dependent kinetic traces and extract k_{CRS} and k_{CRT} from the total observed k_{CR}.[33] Figure 8 outlines the relevant cases that are typically encountered in analyzing the kinetic data, assuming that the RP singlet state is initially populated. The kinetic equations used to obtain the fits have been described recently.[32,33] Three conditions are outlined, $2J \gg a_{eff}$, $2J > a_{eff}$, and $2J \leq a_{eff}$, where a_{eff} is the sum of the hyperfine coupling constants in both radicals, for analyzing the kinetics when $B = 0$, $B = 2J$, and $B \gg 2J$ (Figure 8), and will be described in the context of how the spin-selective rates were extracted for each molecule.

dx.doi.org/10.1021/ja1095649 |J. Am. Chem. Soc. 2011, 133, 3005–3013

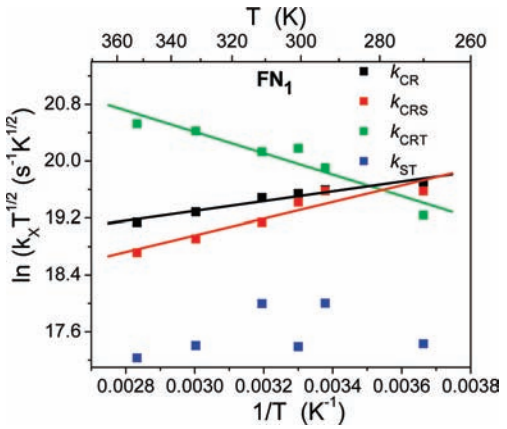

Figure 9. Plot of ln $[k_X T^{1/2}]$ versus $1/T$ for FN_1, where X = CR, CRS, CRT, and ST.

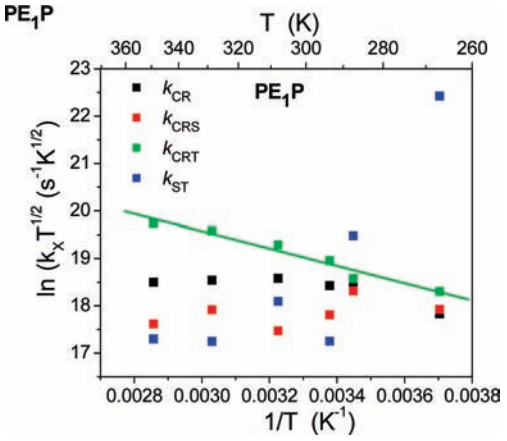

Figure 10. Plot of ln $[k_X T^{1/2}]$ versus $1/T$ for PE_1P, where X = CR, CRS, CRT, and ST.

FN_1 exemplifies the case when $2J \gg a_{eff}$ because $2J = 40$ mT at 295 K and $a_{eff} = 3$ mT.[58,72] When $B = 0$ and $B \gg 2J$, the observed CR kinetics are nearly identical and negligible triplet yields are observed. At magnetic fields far from resonance, the mechanistic scheme simplifies because the observed rate is fast ($1/k_{CR}$ = 54 ns) and the S−T intersystem crossing rate ($1/k_{ST}$) is much slower as a result of the large $2J$ value, so that the apparent decay of the RP should be identical to k_{CRS} (Figure 9). At resonance, $k_{CR} = k_{CRS}/2 + k_{CRT}/2$ because fast intersystem crossing occurs only between S and T_{+1}. Modeling the three kinetic traces at $B = 0$, $B = 2J$, and $B \gg 2J$ using a kinetics simulation based on a matrix formalism,[73] we obtain $1/k_{ST}$ = 261 ns at 295 K (Figure S4). Moreover, a comparison of the analytical and numerical methods gives identical values of k_{CRS} and k_{CRT} for FN_1. In contrast, it is difficult to solve the kinetics analytically for PE_1P, which falls into the intermediate $2J > a_{eff}$ regime (Figure 8), so that the kinetics for PE_1P were solved numerically by fitting them at $B = 0$, $B = 2J$, and $B \gg 2J$ (Figure 10). Last, when $2J \leq a_{eff}$, as it is for FN_2 and PE_2P, it is reasonable to expect a dominant triplet CR pathway because k_{ST} is large, and k_{CRT} is also large because $\Delta G \cong \lambda$. This behavior is observed in the extracted k_{ST} and is shown in Figure 11.

The MFE plots for FN_2 and PE_2P show a low field resonance due to the fact that $2J \leq a_{eff}$ ($2J = 3$ mT at 295 K, Figure S1), and the spin dynamics can be explained in terms of conventional

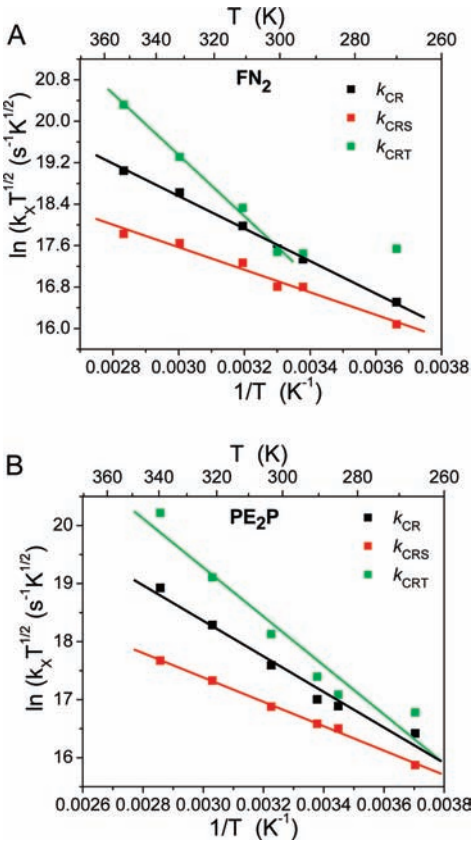

Figure 11. (A) Plot of ln $[k_X T^{1/2}]$ versus $1/T$ for FN_2 and (B) plot of ln $[k_X T^{1/2}]$ versus $1/T$ for PE_2P, where X = CR, CRS, and CRT.

hyperfine and relaxation mechanisms (Figure 8).[74,75] When B = 0, all three RP triplet states are completely mixed with the singlet RP (S) by the hyperfine interaction and the total rate constant, $k_{CR} = 1/4k_{CRS} + 3/4k_{CRT}$. When $B = 2J$, the triplet RP states remain mixed with the singlet state, and only a slight enhancement is observed in the MFE plot. However, when $B \gg 2J$, only the S and T_0 states are fully mixed, and the T_{+1} and T_{-1} states can be ignored; thus, the observed rate constant becomes $k_{CR} = 1/2k_{CRS} + 1/2k_{CRT}$. The hyperfine-driven RP-ISC rate constant, $k_{hfcc} \cong 10^8$ s^{-1}, is much larger than the CR rate constants measured here. A summary of k_{CR}, k_{CRS}, and k_{CRT} obtained using this analysis is given in Table 1.

Temperature Dependence of Charge Recombination. An examination of the CR temperature dependence data for FN_1 (Figure 9) shows that k_{CRS} and k_{CRT} are well described by eq 2. The similarity of the data for k_{CR} and k_{CRS} is explained by the spin dynamics of the RP (see above), which are primarily controlled by the large $2J$ energy gap and result in k_{ST} being relatively small. Interestingly, in this case, a negative activation energy, $\Delta G^{\ddagger} = -811 \pm 147$ cm^{-1}, is observed for k_{CRS}. Because the singlet CR reaction for FN_1 occurs in the Marcus inverted region, k_{CRS} should be only weakly temperature dependent,[26] unless the parameters within eq 2 are also temperature dependent. For example, the temperature dependence of the solvent dielectric constant makes λ_S temperature dependent. In the present case, however, the dielectric constant of toluene decreases only slightly as the temperature is increased over the range measured,[76,77] so that λ_S decreases (see eq S1), and, thus according to eq 2, k_{CRS} should increase slightly, which is

dx.doi.org/10.1021/ja1095649 |J. Am. Chem. Soc. 2011, 133, 3005–3013

contrary to the observed temperature dependence of k_{CRS} (Figure 9).

Negative activation of exergonic electron transfer reactions in a variety of systems has often been attributed to decreasing the population of vibrational states coupled to the reaction coordinate as the temperature is increased.[78−83] With this idea in mind, the negative activation of k_{CRS} can be modeled with a pre-equilibrium mechanism in which increased temperature leads to depletion of the state favorable for electron transfer.[25,31,84−88] In this case, the molecular motions responsible for reactive state depletion are most likely a combination of low-barrier torsions around the single bonds connecting the donor, bridge, and acceptor, as well as vibrations within these components. These dynamics may be represented by a fast equilibrium process between an unreactive RP state $[D^{+\bullet}-B-A^{-\bullet}]$ and a reactive one $[D^{+\bullet}-B-A^{-\bullet}]'$ such that

$$[D^{+\cdot}-B-A^{-\cdot}] \underset{k_{-1}}{\overset{k_1}{\rightleftharpoons}} [D^{+\cdot}-B-A^{-\cdot}]' \xrightarrow{k_2} D-B-A \quad (3)$$

The steady-state solution for the formation of D−B−A in eq 3 yields the observed rate constant k_{CRS} as

$$k_{CRS} = \frac{k_1 k_2}{k_{-1} + k_2} \quad (4)$$

The fact that this process is primarily a tunneling (superexchange) event implies that the actual electron transfer step, k_2, is very slow relative to the motional dynamics. Therefore, $k_{-1} \gg k_2$ and eq 4 reduces to

$$k_{CRS} = K_{eq} k_2 = \exp(-G_{eq}/k_B T) \cdot A_2 \exp(-\Delta G^{\ddagger}_2/k_B T) \quad (5)$$

where $\Delta G_2^{\ddagger}$ is the activation energy for the elementary charge transfer reaction, and ΔG_{eq} is the free energy difference between $[D^{+\bullet}-B-A^{-\bullet}]$ and $[D^{+\bullet}-B-A^{-\bullet}]'$. ΔG_{eq} must be negative if $[D^{+\bullet}-B-A^{-\bullet}]'$ is increasingly depleted at higher temperatures. The observed barrier for singlet CR to ground state, $\Delta G_{CRS}^{\ddagger} = \Delta G_{eq} + \Delta G_2^{\ddagger}$. If ΔG_{eq} is negative and $|\Delta G_{eq}| > \Delta G_2^{\ddagger}$, then $\Delta G_{CRS}^{\ddagger}$ will be negative and k_{CRS} will decrease as temperature increases.

Because $[D^{+\bullet}-B-A^{-\bullet}]' \rightarrow D-B-A$ is an elementary non-adiabatic charge transfer reaction, its rate should be adequately described by eq 2, so that a plot of $\ln k_{CRS} \cdot T^{1/2}$ versus $1/T$ will have slope $-(\Delta G_{eq} + \Delta G_2^{\ddagger})$ as is observed in Figure 9. Furthermore, eq 2 suggests that there are two potential reasons why $[D^{+\bullet}-B-A^{-\bullet}]'$ is the preferred reactive state for singlet CR: (1) the electronic coupling matrix element V_{CRS} for the reaction $[D^{+\bullet}-B-A^{-\bullet}]' \rightarrow D-B-A$ is larger than that for the reaction $[D^{+\bullet}-B-A^{-\bullet}] \rightarrow D-B-A$, and/or (2) $[D^{+\bullet}-B-A^{-\bullet}]'$ has better Franck−Condon overlap with D−B−A than does $[D^{+\bullet}-B-A^{-\bullet}]$.[79−83] If the Franck−Condon overlaps of $[D^{+\bullet}-B-A^{-\bullet}]$ and $[D^{+\bullet}-B-A^{-\bullet}]'$ with D−B−A are similar, a negative activation energy implies that the electronic coupling of $[D^{+\bullet}-B-A^{-\bullet}]$ with D−B−A is larger than that of the reactive state $[D^{+\bullet}-B-A^{-\bullet}]'$ with D−B−A, which is unreasonable. Thus, the temperature dependence of the Franck−Condon factor in eq 2 is most likely responsible for the observed negative activation of CR in FN_1. As the temperature increases, higher-lying, less reactive vibrational states may be populated, which results in a CR rate decrease.

As noted above, the triplet pathway for CR within FN_1 is only accessible when $B = 2J$. Our analysis of k_{CRT} for FN_1 depends on the relationship between V_{CRS}, V_{CRT}, and $2J$ originally proposed by Kramers[89] and developed further by Anderson.[34,90] They concluded that the magnitude and sign of $2J$ depend on the electronic coupling matrix elements of the RP states with other energetically nearby states having the same respective spin multiplicities.[34,90] For the CR reaction, an approximate relationship between $2J$ and the electronic coupling matrix elements for the singlet and triplet pathways, V_{CRS} and V_{CRT}, respectively, is given by eq 6:[37,54,91]

$$2J = \frac{V_{CRS}^2}{\Delta G_{CRS} + \lambda} - \frac{V_{CRT}^2}{\Delta G_{CRT} + \lambda} \quad (6)$$

The measured A factors for CR in FN_1 (and for FN_2 and PE_2P) given in Table 1 are proportional to V_{CR}^2 (eq 2), and these data show that $V_{CRT} \gg V_{CRS}$; thus eq 6 reduces to

$$2J = -\frac{V_{CRT}^2}{\Delta G_{CRT} + \lambda} \quad (7)$$

In our earlier work on FN_{1-3} and $PE_{1-3}P$ at 295 K,[32] we observed that the exponential distance dependences of k_{CRS} and k_{CRT} resulting from the superexchange mechanism of CR are very similar. This was attributed to the counterbalancing effects of the electronic coupling matrix element and the energy gaps between the relevant states. In the work presented here, the fact that $V_{CRT} \gg V_{CRS}$ suggests that the conformational distribution present in the triplet CR differs from that of the singlet pathway. This may be a consequence of the different time scales of CR by these two pathways suggested by their temperature dependence (Figure 9).

Recognizing that ΔG_{CRT} and λ are nearly temperature independent over the range of temperatures measured, resulting largely from the temperature invariance of ε_S for toluene, the observed increase in $2J$ as the temperature is raised (Figure 7) is indicative of an increase in V_{CRT}. This observation correlates well with the fact that k_{CRT}, which is proportional to V_{CRT}^2 (eq 2), displays a positive activation energy in FN_1, $\Delta G^{\ddagger} = 1047 \pm 170$ cm^{-1}, which is nearly identical to that of the bridge torsional frequencies of fluorenyls linked at their 2,7-positions, so that this motion most likely "gates" CR via the triplet pathway.[92,93] Finally, it is important to note that k_{ST} does not change significantly over the temperature range studied (Figure 9), even though at low temperatures, $2J$ decreases due to relaxation of the system into conformations in which the dihedral angles between the π-systems are larger, which diminishes the electronic coupling between them.[68]

Figure 10 shows the results of $\ln(k_X T^{1/2})$ versus $1/T$ for X = CR, CRS, CRT, and ST in PE_1P. Similar to what is observed for FN_1, the triplet pathway displays a positive activation energy, $\Delta G^{\ddagger} = 1368 \pm 285$ cm^{-1} for PE_1P, which corresponds to published *p*-phenylethynylene oligomer rotational barriers.[94] Interestingly, k_{CRS} is temperature independent and qualitatively tracks with k_{CR}. However, a closer evaluation of Figure 5 shows crossover from a singlet temperature-independent pathway to a positively activated triplet pathway near 300 K, which is due to a dramatic increase in the intersystem crossing rate constant, k_{ST}. However, this crossover is not observed in the $2J$ temperature dependence because $2J$ is determined largely by V_{CRT} (eq 7). The activation energy obtained for k_{CRT}, $\Delta G^{\ddagger} = 1269 \pm 131$ cm^{-1}, matches that for the observed rate constant, k_{CR}, over a temperature range of

dx.doi.org/10.1021/ja1095649 |*J. Am. Chem. Soc.* 2011, 133, 3005–3013

270−296 K, for which $\Delta G^{\ddagger}$ = 1368 ± 285 cm^{-1}. The triplet pathway is revealed as the dominant pathway only at lower temperatures, when 2J decreases and k_{ST} increases as a result of changes in the distribution of torsional bridge conformations. Using eqs 2 and S1 with a range of V_{DA} values (0.9−1.4 cm^{-1}) calculated from the experimental 2J values (eq 7) and plotting the data as a function of $1/T$ (from 240 to 360 K, $\Delta G_{CR} = -0.35$, λ_i = 0.39 eV, λ_S = 0.07 eV), the temperature dependence of k_{CRT} is modeled reasonably well (Figures S2 and S3).

The overall observed rates, k_{CR}, for FN_2 and PE_2P show positive activation energies (Figures 4, 5, and 11). In these cases, the spin dynamics allow efficient intersystem crossing from the singlet RP to the triplet RP at low magnetic field strengths, because $2J \approx a_{eff}$. The relative ratio of k_{CRT} and k_{CRS} depends upon V_{CRT}/V_{CRS} as well as the FCWD. In both FN_2 and PE_2P, $k_{CRT} > k_{CR} > k_{CRS}$ (Figure 11), and $\Delta G^{\ddagger}$ for each pathway is listed in Table 1. Once again, the A factors for FN_2 and PE_2P (Table 1) show that $V_{CRT} \gg V_{CRS}$. For FN_2, the torsional barrier for k_{CRT} is nearly 4100 ± 227 cm^{-1} and is similar to the torsional barrier between a flat aromatic molecule and an aromatic imide, which has been calculated to be about 5000 cm^{-1}.[92] Also noteworthy are the activation energies for the singlet pathways of FN_2 and PE_2P, which are both in the range of 1400−1500 cm^{-1}; this is not unexpected because the parameters in eq 2 are nearly identical for these two bridges. Torsional frequencies for the phenyl rings within p-terphenyl[95] are near 1230 cm^{-1}, while those for 2,7-fluorenyl[96] groups are on the order of 1100 cm^{-1}, and p-phenylethynylene oligomers are 870−2443 cm^{-1},[94] and thus correspond well to the activation barriers measured for FN_2 and PE_2P.

CONCLUSIONS

The temperature dependence of charge recombination has been described using semiclassical electron transfer theory. For the molecular bridges studied here, the CR dynamics are complex: the singlet and triplet spin-selective pathways are modulated by spin dynamics that arise from the S−T energy gap (2J) between the singlet and triplet RPs. Analysis of the kinetic data from MFEs provides a powerful tool for elucidating k_{CRS} and k_{CRT} and, in the case for FN_1, reveal that in the absence of a magnetic field the CR dynamics proceed entirely by the Marcus inverted region singlet pathway that is negatively activated and can be described using a pre-equilibrium model. In addition, the corresponding normal region triplet CR dynamics that occur when $B = 2J$ are gated by bridge structural dynamics. For the case of PE_1P, a distinct crossover in CR pathway from singlet to triplet occurs at 300 K that is explained by the temperature dependence of the bridge structural dynamics. For the longer FN_2 and PE_2P bridges, where the triplet pathway dominates at B = 0, CR is "gated" by the torsional barriers around the single bonds linking the 2,7-fluorenone and p-phenylethynylene bridges to the donor and acceptor with activation energies ranging from 1100 to 4500 cm^{-1}. Overall, the data show that using a combination of bridge structures along with application of specific magnetic field strengths can be used to both probe and control CR dynamics, which is an important goal for solar energy conversion and applications in organic electronics.

ASSOCIATED CONTENT

Supporting Information. Additional magnetic field effect data and analysis, simulations based on electron transfer theory, and complete ref 59. This material is available free of charge via the Internet at http://pubs.acs.org.

AUTHOR INFORMATION

Corresponding Author
m-wasielewski@northwestern.edu

ACKNOWLEDGMENT

We would like to thank Dr. Annie Butler Ricks for the synthesis of the D−B−A molecules and Dr. Tomoaki Miura for helpful discussions. This work was supported by the Chemical Sciences, Geosciences, and Biosciences Division, Office of Basic Energy Sciences, DOE, under grant no. DE-FG02-99ER14999.

REFERENCES

(1) Wasielewski, M. R. *Chem. Rev.* **1992**, *92*, 435–461.
(2) Balzani, V.; Credi, A.; Venturi, M. *ChemSusChem* **2008**, *1*, 26–58.
(3) Albinsson, B.; Martensson, J. *J. Photochem. Photobiol., C* **2008**, *9*, 138–155.
(4) Van Vooren, A.; Lemaur, V.; Ye, A. J.; Beljonne, D.; Cornil, J. *ChemPhysChem* **2007**, *8*, 1240–1249.
(5) Goldsmith, R. H.; Vura-Weis, J.; Scott, A. M.; Borkar, S.; Sen, A.; Ratner, M. A.; Wasielewski, M. R. *J. Am. Chem. Soc.* **2008**, *130*, 7659–7669.
(6) Berlin, Y. A.; Burin, A. L.; Ratner, M. A. *Chem. Phys.* **2002**, *275*, 61–74.
(7) Berlin, Y. A.; Hutchison, G. R.; Rempala, P.; Ratner, M. A.; Michl, J. *J. Phys. Chem. A* **2003**, *107*, 3970–3980.
(8) Berlin, Y. A.; Grozema, F. C.; Siebbeles, L. D. A.; Ratner, M. A. *J. Phys. Chem. C* **2008**, *112*, 10988–11000.
(9) Jortner, J.; Bixon, M.; Langenbacher, T.; Michel-Beyerle, M. E. *Proc. Natl. Acad. Sci. U.S.A.* **1998**, *95*, 12759–12765.
(10) Davis, W. B.; Svec, W. A.; Ratner, M. A.; Wasielewski, M. R. *Nature* **1998**, *396*, 60–63.
(11) Albinsson, B.; Eng, M. P.; Pettersson, K.; Winters, M. U. *Phys. Chem. Chem. Phys.* **2007**, *9*, 5847–5864.
(12) Gray, H. B.; Winkler, J. R. *Proc. Natl. Acad. Sci. U.S.A.* **2005**, *102*, 3534–3539.
(13) Lewis, F. D.; Wu, T.; Zhang, Y.; Letsinger, R. L.; Greenfield, S. R.; Wasielewski, M. R. *Science* **1997**, *277*, 673–676.
(14) Kobori, Y.; Yamauchi, S.; Akiyama, K.; Tero-Kubota, S.; Imahori, H.; Fukuzumi, S.; Norris, J. R., Jr. *Proc. Natl. Acad. Sci. U.S.A.* **2005**, *102*, 10017–10022.
(15) Paulson, B. P.; Miller, J. R.; Gan, W.-X.; Closs, G. *J. Am. Chem. Soc.* **2005**, *127*, 4860–4868.
(16) Lembo, A.; Tagliatesta, P.; Guldi, D. M.; Wielopolski, M.; Nuccetelli, M. *J. Phys. Chem. A* **2009**, *113*, 1779–1793.
(17) Wielopolski, M.; Atienza, C.; Clark, T.; Guldi, D. M.; Martin, N. *Chem.-Eur. J.* **2008**, *14*, 6379–6390.
(18) Eng, M. P.; Martensson, J.; Albinsson, B. *Chem.-Eur. J.* **2008**, *14*, 2819–2826.
(19) McConnell, H. M. *J. Chem. Phys.* **1961**, *35*, 508–515.
(20) Paddon-Row, M. N.; Oliver, A. M.; Warman, J. M.; Smit, K. J.; de Haas, M. P.; Oevering, H.; Verhoeven, J. W. *J. Phys. Chem.* **1988**, *92*, 6958–6962.
(21) Roest, M. R.; Oliver, A. M.; PaddonRow, M. N.; Verhoeven, J. W. *J. Phys. Chem. A* **1997**, *101*, 4867–4871.
(22) Lafolet, F.; Welter, S.; Popovic, Z.; De Cola, L. *J. Mater. Chem.* **2005**, *15*, 2820–2828.
(23) Schenck, C. C.; Parson, W. W.; Holten, D.; Windsor, M. W.; Sarai, A. *Biophys. J.* **1981**, *36*, 479–489.
(24) Kroon, J.; Oevering, H.; Verhoeven, J. W.; Warman, J. M.; Oliver, A. M.; Paddon-Row, M. N. *J. Phys. Chem.* **1993**, *97*, 5065–5069.

(25) Weiss, E. A.; Tauber, M. J.; Kelley, R. F.; Ahrens, M. J.; Ratner, M. A.; Wasielewski, M. R. *J. Am. Chem. Soc.* **2005**, *127*, 11842–11850.
(26) Liang, N.; Miller, J. R.; Closs, G. L. *J. Am. Chem. Soc.* **1990**, *112*, 5353–5354.
(27) Smitha, M. A.; Gopidas, K. R. *Chem. Phys. Lett.* **2001**, *350*, 86–92.
(28) Davis, W. B.; Ratner, M. A.; Wasielewski, M. R. *J. Am. Chem. Soc.* **2001**, *123*, 7877–7886.
(29) Goldsmith, R. H.; DeLeon, O.; Wilson, T. M.; Finkelstein-Shapiro, D.; Ratner, M. A.; Wasielewski, M. R. *J. Phys. Chem. A* **2008**, *112*, 4410–4414.
(30) Hoffman, B. M.; Ratner, M. A. *J. Am. Chem. Soc.* **1987**, *109*, 6237–6243.
(31) Weiss, E. A.; Tauber, M. J.; Ratner, M. A.; Wasielewski, M. R. *J. Am. Chem. Soc.* **2005**, *127*, 6052–6061.
(32) Scott, A. M.; Butler Ricks, A.; Colvin, M. T.; Wasielewski, M. R. *Angew. Chem., Int. Ed.* **2010**, *49*, 2904–2908.
(33) Scott, A. M.; Miura, T.; Ricks, A. B.; Dance, Z. E. X.; Giacobbe, E. M.; Colvin, M. T.; Wasielewski, M. R. *J. Am. Chem. Soc.* **2009**, *131*, 17655–17666.
(34) Anderson, P. W. *Phys. Rev.* **1959**, *115*, 2–13.
(35) Shultz, D. A.; Fico, R. M., Jr.; Bodnar, S. H.; Kumar, R. K.; Vostrikova, K. E.; Kampf, J. W.; Boyle, P. D. *J. Am. Chem. Soc.* **2003**, *125*, 11761–11771.
(36) Weiss, E. A.; Ahrens, M. J.; Sinks, L. E.; Gusev, A. V.; Ratner, M. A.; Wasielewski, M. R. *J. Am. Chem. Soc.* **2004**, *126*, 5577–5584.
(37) Kobori, Y.; Sekiguchi, S.; Akiyama, K.; Tero-Kubota, S. *J. Phys. Chem. A* **1999**, *103*, 5416–5424.
(38) Paddon-Row, M. N.; Shephard, M. J. *J. Phys. Chem. A* **2002**, *106*, 2935–2944.
(39) Volk, M.; Haberle, T.; Feick, R.; Ogrodnik, A.; Michel-Beyerle, M. E. *J. Phys. Chem.* **1993**, *97*, 9831–9836.
(40) Weller, A.; Staerk, H.; Treichel, R. *Faraday Discuss. Chem. Soc.* **1984**, *78*, 271–278.
(41) Hoff, A. J.; Gast, P.; van der Vos, R.; Franken, E. M.; Lous, E. J. *Z. Phys. Chem.* **1993**, *180*, 175–192.
(42) Till, U.; Hore, P. J. *Mol. Phys.* **1997**, *90*, 289–296.
(43) Steiner, U. E.; Ulrich, T. *Chem. Rev.* **1989**, *89*, 51–147.
(44) Mori, Y.; Sakaguchi, Y.; Hayashi, H. *J. Phys. Chem. A* **2002**, *106*, 4453–4467.
(45) Blankenship, R. E.; Schaafsma, T. J.; Parson, W. W. *Biochim. Biophys. Acta* **1977**, *461*, 297–305.
(46) Plato, M.; Möbius, K.; Michel-Beyerle, M. E.; Bixon, M.; Jortner, J. *J. Am. Chem. Soc.* **1988**, *110*, 7279–7285.
(47) van der Vos, R.; Hoff, A. J. *Biochim. Biophys. Acta* **1995**, *1228*, 73–85.
(48) Werner, H.-J.; Schulten, K.; Weller, A. *Biochim. Biophys. Acta* **1978**, *502*, 255–268.
(49) Norris, J. R.; Bowman, M. K.; Budil, D. E.; Tang, J.; Wraight, C. A.; Closs, G. L. *Proc. Natl. Acad. Sci. U.S.A.* **1982**, *79*, 5532–5536.
(50) Schulten, K.; Staerk, H.; Weller, A.; Werner, H. J.; Nickel, B. *Z. Phys. Chem.* **1976**, *101*, 371–390.
(51) Tanimoto, Y.; Okada, N.; Itoh, M.; Iwai, K.; Sugioka, K.; Takemura, F.; Nakagaki, R.; Nagakura, S. *Chem. Phys. Lett.* **1987**, *136*, 42–46.
(52) Sakaguchi, Y.; Hayashi, H. *J. Phys. Chem. A* **1997**, *101*, 549–555.
(53) Werner, U.; Kuhnle, W.; Staerk, H. *J. Phys. Chem.* **1993**, *97*, 9280–9287.
(54) Weiss, E. A.; Ratner, M. A.; Wasielewski, M. R. *J. Phys. Chem. A* **2003**, *107*, 3639–3647.
(55) Lukas, A. S.; Bushard, P. J.; Weiss, E. A.; Wasielewski, M. R. *J. Am. Chem. Soc.* **2003**, *125*, 3921–3930.
(56) Tadjikov, B.; Smirnov, S. *Phys. Chem. Chem. Phys.* **2001**, *3*, 204–212.
(57) Tsentalovich, Y. P.; Morozova, O., B.; Avdievich, N. I.; Ananchenko, G. S.; Yurkovskaya, A. V.; Ball, J. D.; Forbes, M. D. E. *J. Phys. Chem. A* **1997**, *101*, 8809–8816.
(58) Dance, Z. E. X.; Ahrens, M. J.; Vega, A. M.; Ricks, A. B.; McCamant, D. W.; Ratner, M. A.; Wasielewski, M. R. *J. Am. Chem. Soc.* **2008**, *130*, 830–832.
(59) Frisch, M. J.; et al. *Gaussian 98*, revision A.97; Gaussian, Inc.: Pittsburgh, PA, 1998. Full reference in the Supporting Information.
(60) Marcus, R. A. *J. Chem. Phys.* **1965**, *43*, 679–701.
(61) Jortner, J. *J. Chem. Phys.* **1976**, *64*, 4860–4867.
(62) Hopfield, J. J. *Proc. Natl. Acad. Sci. U.S.A.* **1974**, *71*, 3640–3644.
(63) Wiederrecht, G. P.; Svec, W. A.; Wasielewski, M. R.; Galili, T.; Levanon, H. *J. Am. Chem. Soc.* **2000**, *122*, 9715–9722.
(64) Ganesan, P.; Baggerman, J.; Zhang, H.; Sudhoelter, E. J. R.; Zuilhof, H. *J. Phys. Chem. A* **2007**, *111*, 6151–6156.
(65) Langelaar, J.; Rettschnick, R. P. H.; Hoijtink, G. J. *J. Chem. Phys.* **1971**, *54*, 1–7.
(66) Livingston, R.; Tanner, D. W. *Trans. Faraday Soc.* **1958**, *54*, 765–771.
(67) Greenfield, S. R.; Svec, W. A.; Gosztola, D.; Wasielewski, M. R. *J. Am. Chem. Soc.* **1996**, *118*, 6767–6777.
(68) Dance, Z. E. X.; Mi, Q.; McCamant, D. W.; Ahrens, M. J.; Ratner, M. A.; Wasielewski, M. R. *J. Phys. Chem. B* **2006**, *110*, 25163–25173.
(69) Closs, G. L.; Forbes, M. D. E.; Norris, J. R. *J. Phys. Chem.* **1987**, *91*, 3592–3599.
(70) Hore, P. J.; Hunter, D. A.; McKie, C. D.; Hoff, A. J. *Chem. Phys. Lett.* **1987**, *137*, 495–500.
(71) Miura, T.; Scott, A. M.; Wasielewski, M. R. *J. Phys. Chem. C* **2010**, *114*, 20370–20379.
(72) Dance, Z. E. X.; Mickley, S. M.; Wilson, T. M.; Ricks, A. B.; Scott, A. M.; Ratner, M. A.; Wasielewski, M. R. *J. Phys. Chem. A* **2008**, *112*, 4194–4201.
(73) Murakami, M.; Maeda, K.; Arai, T. *J. Phys. Chem. A* **2005**, *109*, 5793–5800.
(74) Steiner, U. E.; Ulrich, T. *Chem. Rev.* **1989**, *89*, 51–147.
(75) Hayashi, H. *Introduction to Dynamic Spin Chemistry: Magnetic Field Effects upon Chemical and Biochemical Reactions*; World Scientific: Singapore, 2004.
(76) Mopsik, F. I. *J. Chem. Phys.* **1969**, *50*, 2559–2569.
(77) Ritzoulis, G.; Papadopoulos, N.; Jannakoudakis, D. *J. Chem. Eng. Data* **1986**, *31*, 146–148.
(78) Parson, W. W. *Biochim. Biophys. Acta* **1967**, *131*, 154–172.
(79) Buhks, E.; Jortner, J. *FEBS Lett.* **1980**, *109*, 117–120.
(80) Vauthey, E.; Suppan, P. *Chem. Phys.* **1989**, *139*, 381–390.
(81) Woodbury, N. W.; Becker, M.; Middendorf, D.; Parson, W. W. *Biochemistry* **1985**, *24*, 7516–7521.
(82) Bixon, M.; Jortner, J.; Michel-Beyerle, M. E. *Biochim. Biophys. Acta* **1991**, *1056*, 301–315.
(83) Scherer, P. O. J.; Fischer, F. *Chem. Phys. Lett.* **1987**, *141*, 179–185.
(84) Kiselev, V. D.; Miller, J. R. *J. Am. Chem. Soc.* **1975**, *97*, 4036–4039.
(85) Zaman, K. M.; Yamamoto, S.; Nishimura, N. *J. Am. Chem. Soc.* **1994**, *116*, 12099–12100.
(86) Yamamoto, S.; Sakurai, T.; Yingjin, L.; Sueishi, Y. *Phys. Chem. Chem. Phys.* **1999**, *1*, 833–837.
(87) Fukuzumi, S.; Ohkubo, K.; Tokuda, Y.; Suenobu, T. *J. Am. Chem. Soc.* **2000**, *122*, 4286–4294.
(88) Frank, R.; Greiner, G.; Rau, H. *Phys. Chem. Chem. Phys.* **1999**, *1*, 3841–3490.
(89) Kramers, H. A. *Physica* **1934**, *1*, 182–192.
(90) Anderson, P. W. *Phys. Rev.* **1950**, *79*, 350–356.
(91) Nelsen, S. F.; Ismagilov, R. F.; Teki, Y. *J. Am. Chem. Soc.* **1998**, *120*, 2200–2201.
(92) Cui, C. Z.; Cho, S. J.; Kim, K. S.; Baehr, C.; Jung, J. C. *J. Chem. Phys.* **1997**, *107*, 10201–10206.
(93) Wilson, N. K. *Magn. Reson. Chem.* **1985**, *23*, 12–15.
(94) Ricca, A.; Bauschlicher, C. W. *J. Phys. Chem. B* **2005**, *109*, 9059–9065.
(95) Tekely, P.; Laupretre, F.; Monnerie, L. *Macromolecules* **1983**, *16*, 415–420.
(96) Prins, P.; Grozema, F. C.; Galbrecht, F.; Scherf, U.; Siebbeles, L. D. A. *J. Phys. Chem. C* **2007**, *111*, 11104–11112.